Activation of Carbon Dioxide: Gas-Phase Reactions of Y^+, YO^+, and YO_2^+ with CO and CO_2

M. R. Sievers and P. B. Armentrout*

Department of Chemistry, University of Utah, Salt Lake City, Utah 84112

Received September 17, 1998

Insight into the fundamental character of carbon dioxide activation at metal centers is studied in the gas phase using guided ion beam mass spectrometry. The reactions of Y^+ and YO^+ with CO_2 and the reverse reactions, YO^+ and YO_2^+ with CO, are investigated. To probe the potential energy surfaces of these systems more completely, YO_2^+ and the complexes $OY(CO_2)^+$, $OY(CO)^+$, and $O_2Y(CO)^+$ are studied by collisional activation experiments with Xe. Thermochemical analysis of the reaction cross sections obtained in this study yield (in eV) $D_0(Y^+-CO) = 0.31 \pm 0.11$, $D_0(OY^+-CO) = 0.71 \pm 0.04$, $D_0(O_2Y^+-CO) = 0.69 \pm 0.03$, and $D_0(OY^+-CO_2) = 0.89 \pm 0.05$.

I. Introduction

In recent work, we have examined the gas-phase reactions of several atomic metal ions and diatomic metal oxide ions with carbon monoxide and carbon dioxide.[1−4] One purpose of such work is to help provide insight and thermodynamic information regarding the fundamental interactions of metals with such gases. Such insight may be useful in better understanding the use of metal and metal oxide catalysts to convert carbon dioxide and carbon monoxide to more useful chemical materials.[5−14] Previously, several groups have used ion cyclotron resonance (ICR) mass spectrometry to study the gas-phase interactions of CO_2 with metal cations and metal oxide cations at thermal energies.[15−21] In our work, we have used guided ion beam mass spectrometry to examine the following reaction systems in detail:

$$M^+ + CO_2 \rightarrow MO^+ + CO \quad (1)$$

for M = V,[1] Nb, NbO,[2] Zr, ZrO,[3] Mo, and MoO.[4] We observed complex cross section energy dependencies for these reaction systems. Analyses of these cross sections resulted in the determination of thermochemistry and electronic excitation energies for VO^+ and NbO^+ that agreed well with previously reported values obtained in photoelectron studies of VO and NbO by Dyke et al.[22,23] In other systems where no literature information was available, we speculatively assigned excitation energies for additional states of NbO^+, NbO_2^+, ZrO^+, MoO^+, and MoO_2^+. In addition, thermochemistries for several $M^+(CO)$ and $M^+(CO_2)$ species were determined. The present work extends these detailed studies to M = Y and YO.

Efficient oxidation of CO to CO_2 at thermal energies requires that the species donating the oxygen atom must have a bond dissociation energy (BDE) less than 5.45 eV = $D_0(OC-O)$.[24] Previous work performed in our laboratories has determined $D_0(Y^+-O) = 7.24 \pm 0.18$ eV[25] and $D_0(OY^+-O) = 1.76 \pm 0.16$ eV[26] (Table 1). Thus reaction 1 is exothermic for M = Y, while the reverse process is exothermic for M = YO.

II. Experimental Section

A. General Procedures. These studies are performed using a guided ion beam tandem mass spectrometer. The instrument and experimental methods have been described previously.[27,28] Ions, formed as described below, are extracted from the source, accelerated, and focused into a magnetic sector momentum analyzer for mass analysis. The ions are decelerated to a desired kinetic energy and focused into an octopole

(1) Sievers, M. R.; Armentrout, P. B. *J. Chem. Phys.* **1995**, *102*, 754.
(2) Sievers, M. R.; Armentrout, P. B. *Int. J. Mass Spectrom.* **1998**, *179*/*180*, 103.
(3) Sievers, M. R.; Armentrout, P. B. *Int. J. Mass Spectrom.*, in press.
(4) Sievers, M. R.; Armentrout, P. B. *J. Phys. Chem. A*, accepted for publication.
(5) Avila, Y.; Barrault, J.; Pronier, S.; Kappenstein, C. *Appl. Catal. A* **1995**, *132*, 97.
(6) Miciukiewicz, J.; Mang, T. *Appl. Catal. A* **1995**, *122*, 151.
(7) Fujita, T.; Nishiyama, Y.; Ohtsuka, Y.; Asami, K.; Kusakabe, K.-I. *Appl. Catal. A* **1995**, *126*, 245.
(8) Weimer, T.; Schaber, K.; Specht, M.; Bandi, A. *Energy Convers. Manage.* **1996**, *37*, 1351.
(9) Yanagisawa, Y. *Energy Convers. Manage.* **1995**, *36*, 443.
(10) Park, S.-E.; Nam, S. S.; Choi, M. J.; Lee, K. W. *Energy Convers. Manage.* **1995**, *36*, 573.
(11) Saito, M.; Fujitani, T.; Takahara, I.; Watanabe, T.; Takeuchi, M.; Kanai, Y.; Moriya, K.; Kakumoto, T. *Energy Convers. Manage.* **1995**, *36*, 577.
(12) Hirano, M.; Akano, T.; Imai, T.; Kuroda, K. *Energy Convers. Manage.* **1995**, *36*, 585.
(13) Otorbaev, D. K. *Chem. Phys.* **1995**, *196*, 543.
(14) Sahibzada, M.; Chadwick, D.; Metcalfe, I. S. *Catal. Today* **1996**, *29*, 367.
(15) Kappes, M. M.; Staley, R. H. *J. Phys. Chem.* **1981**, *85*, 942.
(16) Kappes, M. M.; Staley, R. H. *J. Am. Chem. Soc.* **1981**, *103*, 1286.
(17) Kikthenko, A. V.; Goncharov, V. B.; Zamaraev, K. I. *Catal. Lett.* **1993**, *21*, 353.
(18) Izod, T. P. J.; Kistiakowsky, G. B.; Matsuda, S. *J. Chem. Phys.* **1972**, *76*, 2833.
(19) Matsuda, S. *J. Chem. Phys.* **1972**, *57*, 807.
(20) Matsuda, S. *J. Phys. Chem.* **1972**, *76*, 2833.
(21) Wesendrup, R.; Schwarz, H. *Angew. Chem., Int. Ed. Engl.* **1995**, *34*, 2033.
(22) Dyke, J. M.; Gravenor, W. J.; Hastings, M. P.; Morris, A. *J. Phys. Chem.* **1985**, *89*, 4613.
(23) Dyke, J. M.; Ellis, A. M.; Fehér, M.; Morris, A.; Paul, A. J.; Stevens, J. C. H. *J. Chem. Soc., Faraday Trans. 2* **1987**, *83*, 1555.
(24) Calculated from data in: Lias, S. G.; Bartmess, J. E.; Liebman, J. F.; Holmes, J. L.; Levin, R. D.; Mallard, W. G. *J. Phys. Chem. Ref. Data* **1988**, *17*, Suppl. No. 1.
(25) Sievers, M. R.; Chen, Y.-M.; Armentrout, P. B. *J. Chem. Phys.* **1996**, *105*, 6322.
(26) Clemmer, D. E.; Dalleska, N. F.; Armentrout, P. B. *Chem. Phys. Lett.* **1992**, *190*, 259.
(27) Ervin, K. M.; Armentrout, P. B. *J. Chem. Phys.* **1985**, *83*, 166.
(28) Schultz, R. H.; Armentrout, P. B. *Int. J. Mass Spectrom. Ion Processes* **1991**, *107*, 29.

10.1021/ic981117f CCC: $18.00
Published on Web 01/06/1999

Table 1. Bond Dissociation Energies at 0 K

bond	bond energy (eV)
C−O	11.108 ± 0.005[a]
OC−O	5.453 ± 0.002[a]
Y^+−O	7.24 ± 0.18[b]
Y^+−CO	0.42 ± 0.13,[c] 0.31 ± 0.11[d]
OY^+−O	1.76 ± 0.16,[c] 1.4 ± 0.5[d]
OY^+−CO	0.71 ± 0.04[d]
OY^+−CO_2	0.89 ± 0.05[d]
O_2Y^+−CO	0.69 ± 0.03[d]

[a] Ref 24. [b] Ref 25. [c] Ref 42. [d] This work. [e] Ref 26.

ion guide that radially traps the ions. While in the octopole, the ions pass through a gas cell that contains the neutral reactant at pressures where multiple collisions are improbable (<0.30 mTorr). Single-collision conditions were verified by examining the pressure dependence of the cross sections measured here. The product ions and the reactant ion beam drift out of the gas cell, are focused into a quadrupole mass filter, and then detected by a secondary electron scintillation detector. Ion intensities are converted to absolute cross sections as described previously.[27] Uncertainties in the absolute cross sections are estimated at ±20%.

To determine the absolute zero and distribution of the ion kinetic energy, the octopole is used as a retarding energy analyzer.[27] The uncertainty in the absolute energy scale is ±0.05 eV (lab). The full width at half-maximum (fwhm) of the ion energy distribution is 0.2−0.4 eV (lab). Lab energies are converted into center-of-mass energies using $E(\mathrm{CM}) = E(\mathrm{lab})m/(m + M)$, where M and m are the masses of the ion and neutral reactant, respectively. All energies stated in this paper are in the center-of-mass frame, unless noted otherwise.

B. Ion Source. The ion source used here is a dc discharge/flow tube (DC/FT) source described in previous work.[23] The DC/FT source utilizes a tantalum cathode with a cavity that contains yttrium chloride salt. The cathode is held at 1.5−3 kV. A flow of approximately 90% He and 10% Ar passes over the cathode at a typical pressure of ∼0.5 Torr. Ar^+ ions created in a direct current discharge are accelerated toward the cathode, sputtering off atomic metal ions. The ions then undergo $\sim 10^5$ collisions with He and $\sim 10^4$ collisions with Ar in the meter long flow tube before entering the guided ion beam apparatus. From previous studies of Y^+ reactions,[29] we believe that the Y^+ ions produced in the DC/FT source are exclusively in their a^1S ground state.

Ground-state YO^+ and YO_2^+ were made by allowing Y^+ (created in the dc discharge) to react with O_2 introduced ∼25 cm downstream into the flow tube at ∼2 mTorr. $OY^+(CO)$ and O_2YCO^+ were produced by allowing the Y^+ to react with O_2 upstream in the flow tube and CO downstream. $OY^+(CO_2)$ was produced by allowing the YO^+ to interact with CO_2 downstream in the flow tube. Three-body collisions with the He/Ar flow gas stabilize these complex species. The large number of collisions between the ions and the bath gases should thermalize these polyatomic ions both rotationally and vibrationally. We assume that these ions are in their ground electronic states and that the internal energy of these clusters is well described by a Maxwell−Boltzmann distribution of rotational and vibrational states corresponding to 300 K. Previous work from this laboratory, including studies of N_4^+,[30] $Fe(CO)_x^+$ ($x = 1-5$),[31] $Cr(CO)_x^+$ ($x = 1-6$),[32] SiF_x^+ ($x = 1-4$),[33] and $H_3O^+(H_2O)_x$ ($x = 1-5$),[34] has shown that these assumptions are usually valid.

Attempts were made to produce $Y^+(CO_2)$. Addition of CO_2 downstream in the flow tube did produce a cation which had the mass of $Y^+(CO_2)$. However, preliminary CID experiments performed on this cation indicated that the ion was in fact $OY^+(CO)$ and not the CO_2 ligated yttrium cation. In addition, ligand exchange reactions between $Y^+(N_2)$ and CO_2 in the flow tube did not form any of the $Y^+(CO_2)$ complex.

Table 2. Molecular Vibrational Frequencies

species		frequencies (degeneracies), cm^{-1}
YO^+[a]		1076
YO_2^+[a]		441, 716, 846
CO_2[b]		667(2), 1333, 2349
CO[c]		2214.2
$OY^+(CO)$	(1)[a]	35(2), 166, 221(2) + $\nu(YO^+)$ + ν(CO)
	(2)[a]	20(2), 100, 150(2) + $\nu(YO^+)$ + ν(CO)
$OY^+(CO_2)$	(1)[a]	150(2), 200(2) + $\nu(YO^+)$ + $\nu(CO_2)$
	(2)[d]	25, 105, 196, 200, 600, 935, 1076, 1176, 1745
$O_2Y^+(CO)$	(1)[a]	20(2), 100, 150(2) + $\nu(YO_2^+)$ + ν(CO)
	(2)[a]	35(2), 166, 221(2) + $\nu(YO_2^+)$ + ν(CO)

[a] See text for details. [b] Ref 38. [c] Ref 39. [d] $V^+(CO_2)$ frequencies from ref 1 and estimates for two bends (25 and 200 cm^{-1}).

C. Data Analysis. Previous theoretical[35,36] and experimental work[37] has shown that endothermic cross sections can be modeled using eq 2,

$$\sigma(E) = \sigma_0 \sum g_i (E + E_{\mathrm{rot}} + E_i - E_0)^n / E \qquad (2)$$

where σ_0 is an energy-independent scaling parameter, E is the relative translational energy of the reactants, E_{rot} is the average rotational energy of the reactants, E_0 is the reaction threshold at 0 K, and n is an energy-independent scaling parameter. The summation is over each vibrational state of the reactants having relative populations g_i and energies E_i. The various sets of vibrational frequencies used are listed in Table 2. The frequencies for CO and CO_2 are well established.[38,39] The vibrational frequency for YO^+ was estimated by scaling that for NbO^+ with a Morse potential.[23] The frequencies for YO_2^+ were estimated by scaling those for NbO_2 determined by electron diffraction with a Morse potential.[40] We also assume the geometry of the dioxide cation is nonlinear as for NbO_2^+. The vibrational frequencies for $OY^+(CO)$, $O_2Y^+(CO)$, and $OY^+(CO_2)$ were taken to equal the vibrational frequencies of YO^+ or YO_2^+, and CO or CO_2, plus sets of frequencies for the O_xY^+−CO or OY^+−CO_2 modes that are similar to those we have used previously for $CrCO^+$ [32] and $V^+(CO_2)$.[1] All frequencies used in this study are estimates and therefore were varied by ±20%.

Before comparison with the data, the model of eq 2 is convoluted over the neutral and ion kinetic energy distributions using previously developed methods.[27] The parameters E_0, σ_0, and n are then optimized by using a nonlinear least-squares analysis in order to best reproduce the data. Reported values of E_0, σ_0, and n are mean values for each parameter from the best fits to several independent sets of data, and uncertainties are one standard deviation from the mean. The listed uncertainty in E_0 also includes the uncertainty in the absolute energy scale and uncertainties introduced by the estimated vibrational frequencies used for the various complexes studied.

III. Results

A. $Y^+ + CO_2$. Yttrium cations react with carbon dioxide to form two ionic products in reactions 3 and 4, as shown in Figure 1.

(29) Sievers, M. R.; Chen, Y.-M.; Elkind, J. L.; Armentrout, P. B. *J. Phys. Chem.* **1996**, *100*, 54.
(30) Schultz, R. H.; Armentrout, P. B. *J. Chem. Phys.* **1992**, *96*, 1046.
(31) Schultz, R. H.; Crellin, K. C.; Armentrout, P. B. *J. Am. Chem. Soc.* **1992**, *113*, 8590.
(32) Khan, F. A.; Clemmer, D. E.; Schultz, R. H.; Armentrout, P. B. *J. Phys. Chem.* **1993**, *97*, 7978.
(33) Fisher, E. R.; Kickel, B. L.; Armentrout, P. B. *J. Phys. Chem.* **1993**, *97*, 10204.
(34) Dalleska, N. F.; Honma, K.; Armentrout, P. B. *J. Am. Chem. Soc.* **1993**, *115*, 12125.
(35) Aristov, N.; Armentrout, P. B. *J. Am. Chem. Soc.* **1986**, *108*, 1806, and references therein.
(36) Chesnavich, W. J.; Bowers, M. T. *J. Phys. Chem.* **1979**, *83*, 900.
(37) Armentrout, P. B. In *Advances in Gas-Phase Ion Chemistry*, Vol. 1; Adams, N. G., Babcock, L. M., Eds.; JAI: Greenwich, 1992; pp 83−119.
(38) Shimanouchi, T. *Table of Molecular Vibrational Frequencies*, Consolidated, Vol. I; National Bureau of Standards: Washington, DC, 1972.
(39) Huber, K. P.; Herzberg, G. *Molecular Spectra and Molecular Structure IV. Constants of Diatomic Molecules*, Vol. IV; Van Nostrand Reinhold Co.: New York, 1979.
(40) Gershikov, A. G.; Spiridonov, V. P.; Prikhod'ko, A. Ya.; Erokhin, E. V. *High Temp. Sci.* **1981**, *14*, 17.

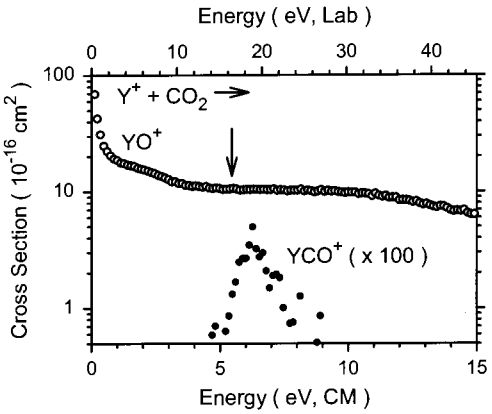

Figure 1. Product cross sections for the reaction of $Y^+ + CO_2$ as a function of collision energy in the center-of-mass frame (lower *x* axis) and laboratory frame (upper *x* axis). The arrow marks the bond dissociation energy of CO_2 at 5.45 eV.

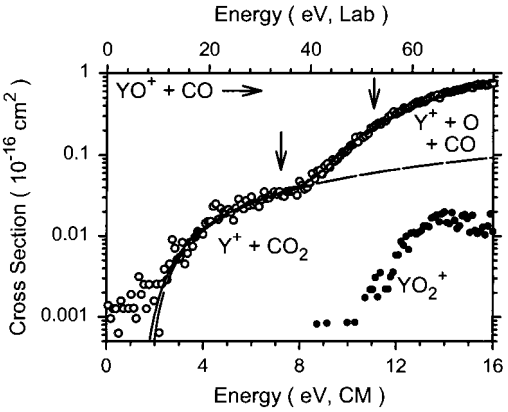

Figure 2. Product cross sections for the reaction of $YO^+ + CO$ as a function of collision energy in the center-of-mass frame (lower *x* axis) and laboratory frame (upper *x* axis). Arrows mark the bond dissociation energies of YO^+ at 7.24 eV and CO at 11.11 eV. The dashed lines are the models of eq 2 with the optimized parameters listed in Table 3 for formation of $Y^+(^1S) + CO_2$ and simple CID of YO^+. The solid line is the sum of the models convoluted with the experimental energy distributions.

$$Y^+ + CO_2 \rightarrow YO^+ + CO \quad (3)$$

$$\rightarrow YCO^+ + O \quad (4)$$

Under the single-collision conditions appropriate for the data in Figure 1 (and all remaining data plots), intermediates such as $Y^+(CO_2)$ and $OY^+(CO)$ are not observed, as these species have enough energy to dissociate to products or return to reactants (in contrast to the situation in the flow tube source, where such complexes can be stabilized by collisions with the high-pressure flow gases present). Literature thermochemistry (Table 1) establishes that reaction 3 is exothermic by 1.79 ± 0.18 eV. The YO^+ cross section does show exothermic reaction behavior up to near 1 eV. At these low energies, the data can be reproduced by scaling the collision cross section,[41] which declines as $E^{-0.5}$, by 0.64. Thus, YO^+ is formed in roughly two of every three collisions. The cross section then declines somewhat less rapidly to near 5 eV, where it remains fairly constant until near 8 eV, at which point it begins to slowly decline.

The formation of YCO^+ begins near 5 eV. Analysis of this cross section with eq 2 yields an E_0 value of 5.14 ± 0.11 eV, which corresponds to $D_0(Y^+-CO) = 0.31 \pm 0.11$ eV (Table 1). This is in reasonable agreement with a calculated bond energy of 0.42 ± 0.13 eV.[42] This cross section reaches a maximum near $D_0(OC-O)$, indicating that its decline is due to reaction 5, dissociation of the YCO^+ product.

$$Y^+ + CO_2 \rightarrow Y^+ + CO + O \quad (5)$$

The elevated threshold and competition with the much more favorable reaction 3 explains the small size of the cross section for reaction 4.

B. $YO^+ + CO$. The reaction of YO^+ and CO, shown in Figure 2, forms two different ionic products in reactions 6−8.

$$YO^+ + CO \rightarrow Y^+ + O + CO \quad (6)$$

$$\rightarrow Y^+ + CO_2 \quad (7)$$

$$\rightarrow YO_2^+ + C \quad (8)$$

The Y^+ cross section slowly rises from an apparent threshold near 1 eV until near 8 eV, at which point it increases more rapidly. The latter feature corresponds to reaction 6, simple collision-induced dissociation, which can begin at $D_0(Y^+-O)$ (Table 1). Thus, the lower energy feature must be due to reaction 7, the reverse of reaction 3, and is endothermic by 1.79 ± 0.18 eV (Table 1). Modeling of this lower energy feature with eq 2 gives an E_0 value of 1.68 ± 0.26 eV (Table 3), which compares very favorably with the predicted threshold. Modeling of the higher energy feature gives an E_0 value of 8.5 ± 0.4 eV, comparable to the 8.02 ± 0.25 eV value obtained from simple CID of YO^+ with Xe.[25] These thresholds are slightly higher than the YO^+ BDE determined from analysis of the reaction of Y^+ with CO (Table 1). This is typical CID behavior for such strongly bound species.[25,43]

The YO_2^+ cross section rises from an apparent threshold near 10 eV until reaching a maximum near 14 eV. Modeling of this cross section gives an E_0 value of 10.47 ± 0.33 eV (Table 3), higher than the thermodynamic threshold of 9.34 ± 0.16 eV (Table 1). It seems likely that this is primarily because of competition with the much more favorable processes forming Y^+.

C. $YO^+ + CO_2$. Two ionic products are observed in the reaction of YO^+ with CO_2, as shown in Figure 3. These can be formed in reactions 9 and 10.

$$YO^+ + CO_2 \rightarrow YO_2^+ + CO \quad (9)$$

$$\rightarrow Y^+ + CO_2 + O \quad (10)$$

Literature thermochemistry (Table 1) predicts that the formation of the dominant product at low energies, YO_2^+, is endothermic by 3.69 ± 0.16 eV. The YO_2^+ product cross section does show endothermic reaction behavior with an apparent threshold near 5 eV. The cross section continues to rise until near 11 eV, at which point it starts to decline with increasing energy. This decline appears to be a consequence of competition with the more favorable process at high energies, reaction 10. Analysis of this cross section with eq 2 results in an E_0 value of 4.54 ± 0.30 eV. The elevated threshold observed in this case is discussed below.

The Y^+ cross section rises from an apparent threshold near 8 eV and continues to rise rapidly. Analysis of this cross section

(41) Gioumousis, G.; Stevenson, D. P. *J. Chem. Phys.* **1958**, *29*, 294.
(42) Barnes, L. A.; Rosi, M.; Bauschlicher, C. W., Jr. *J. Chem. Phys.* **1990**, *93*, 609.

Table 3. Optimized Parameters of eq 2 for YCO_2^+ and YCO_3^+ Systems

reaction	σ_0	n	E_0, eV
(4) $Y^+ + CO_2 \rightarrow YCO^+ + O$	0.34 (0.08)	1.8 (0.3)	5.14 (0.11)
(7) $YO^+ + CO \rightarrow Y^+ + CO_2$	0.011 (0.004)	1.9 (0.2)	1.68 (0.26)
(6) $\rightarrow Y^+ + O + CO$	0.35 (0.19)	1.8 (0.3)	8.5 (0.4)
(8) $\rightarrow YO_2^+ + C$	0.025 (0.014)	2.0 (0.4)	10.47 (0.33)
(9) $YO^+ + CO_2 \rightarrow YO_2^+ + CO$	0.017 (0.007)	1.7 (0.2)	4.54 (0.30)
(10) $\rightarrow Y^+ + O + CO_2$	0.027 (0.016)	2.6 (0.2)	8.10 (0.33)
(11) $YO_2^+ + CO \rightarrow YO^+ + CO_2$	0.23 (0.04)	1.3 (0.2)	0.38 (0.11)
(12) $\rightarrow YO^+ + CO + O$	1.61 (0.49)	1.8 (0.2)	3.39 (0.16)
(13) $OY^+(CO) + Xe \rightarrow YO^+ + CO + Xe$	33.6 (1.3)	1.1 (0.2)	0.71 (0.04)
(14) $OY^+(CO_2) + Xe \rightarrow YO^+ + CO_2 + Xe$	19.5 (0.9)	1.0 (0.2)	0.89 (0.05)
(15) $O_2Y^+(CO) + Xe \rightarrow YO_2^+ + CO + Xe$	55.4 (2.5)	1.0 (0.2)	0.69 (0.03)
(16) $YO_2^+ + Xe \rightarrow YO^+ + O + Xe$	0.25 (0.11)	1.9 (0.2)	1.4 (0.5)

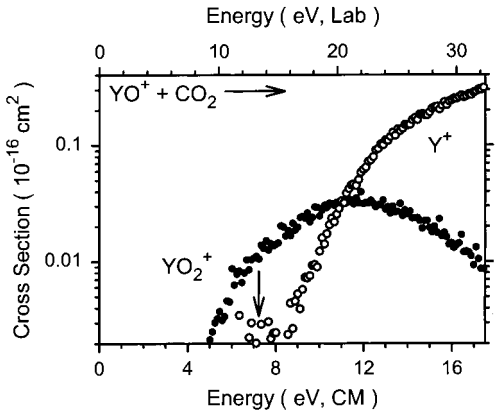

Figure 3. Product cross sections for the reaction of $YO^+ + CO_2$ as a function of collision energy in the center-of-mass frame (lower *x* axis) and laboratory frame (upper *x* axis). The arrow marks the bond dissociation energy of YO^+ at 7.24 eV.

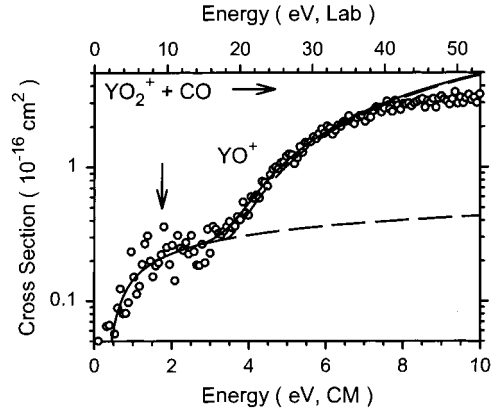

Figure 4. Product cross sections for the reaction of $YO_2^+ + CO$ as a function of collision energy in the center-of-mass frame (lower *x* axis) and laboratory frame (upper *x* axis). The arrow marks the bond dissociation energy of YO_2^+ at 1.76 eV. The dashed lines are the models of eq 2 with the optimized parameters listed in Table 3. The solid line is the sum of the models convoluted with the experimental energy distributions.

yields an E_0 value (Table 3) that is consistent with results obtained from the CID of YO^+ by Xe.[25] As for the case with CID by CO, the threshold is somewhat higher than the thermodynamic value for the YO^+ BDE (Table 1).

D. $YO_2^+ + CO$. The reaction of YO_2^+ with CO results in the formation of one ionic product, shown in Figure 4, that can be formed in reactions 11 and 12.

$$YO_2^+ + CO \rightarrow YO^+ + CO_2 \quad (11)$$

$$\rightarrow YO^+ + CO + O \quad (12)$$

The YO^+ cross section rises from an apparent threshold near 0.5 eV and then plateaus. Near 3 eV, the YO^+ cross section rises sharply until near 8 eV, at which point it begins to level off. Literature thermochemistry (Table 1) predicts that reaction 11 is exothermic by 3.69 ± 0.16 eV and that reaction 12 can start at 1.76 ± 0.16 eV (Table 1). Therefore, the low-energy feature in this cross section must be due to reaction 11, but it is very inefficient considering that formation of ground-state YO^+ ($^1\Sigma^+$) + CO_2 ($^1\Sigma_g^+$) products is exothermic. The observation of a barrier in this case is discussed below.

The higher energy feature in this cross section is almost certainly a result of simple CID, reaction 12, as the shape and magnitude of the cross section are similar to that for CID of YO_2^+ with Xe (section E). In this case, the apparent threshold and our measured value for E_0 (Table 3) lie well above the thermodynamic limit. It should be realized that this analysis is highly dependent on the assumptions made about the shape of the cross section for reaction 11, which are reasonable but may not be accurate. Clearly, our sensitivity to the real threshold for reaction 12 suffers because of the presence of the lower energy channel.

E. Collision-Induced Dissociation Studies. To further characterize possible intermediates in the YCO_2^+ and YCO_3^+ systems, we also generated $OY^+(CO)$, $OY^+(CO_2)$, $O_2Y^+(CO)$, and YO_2^+ species and collisionally activated them with Xe. In the first three cases, the only ionic product observed is the loss of the ligand, i.e., reactions 13, 14, and 15.

$$OY^+(CO) + Xe \rightarrow YO^+ + CO + Xe \quad (13)$$

$$OY^+(CO_2) + Xe \rightarrow YO^+ + CO_2 + Xe \quad (14)$$

$$O_2Y^+(CO) + Xe \rightarrow YO_2^+ + CO + Xe \quad (15)$$

Results for the two YCO_3^+ isomers are shown in Figures 5 and 6. These observations verify the structures written for each system. Further, if $O_2Y^+(CO)$ had a structure of molecular oxygen bound to Y^+, i.e., $Y^+(O_2)(CO)$, then we would anticipate seeing competitive loss of O_2. Failure to observe this process points to a covalently bound yttrium dioxide cation. In all cases, the cross sections rise from apparent thresholds near 0.5 eV and continue to increase until near 1−1.5 eV, where they plateau. Analysis of these cross sections using eq 2 yields E_0 values for these processes of 0.71 ± 0.04, 0.89 ± 0.05, and 0.69 ± 0.03 eV, respectively (Table 3). These values are assigned to $D_0(OY^+-CO)$, $D_0(OY^+-CO_2)$, and $D_0(O_2Y^+-CO)$.

Collision-induced dissociation of YO_2^+ with Xe gives only one ionic product in reaction 16, as shown in Figure 7.

$$YO_2^+ + Xe \rightarrow YO^+ + O + Xe \quad (16)$$

No Y^+ formation is observed, indicating that YO_2^+ has a dioxide

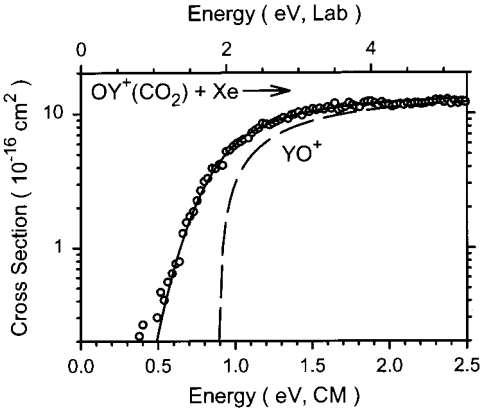

Figure 5. Product cross sections for $OY^+(CO_2) + Xe$ as a function of collision energy in the center-of-mass frame (lower *x* axis) and laboratory frame (upper *x* axis). The dashed line is the model of eq 2 with the optimized parameters listed in Table 3. The solid line shows the model convoluted with the experimental energy distributions.

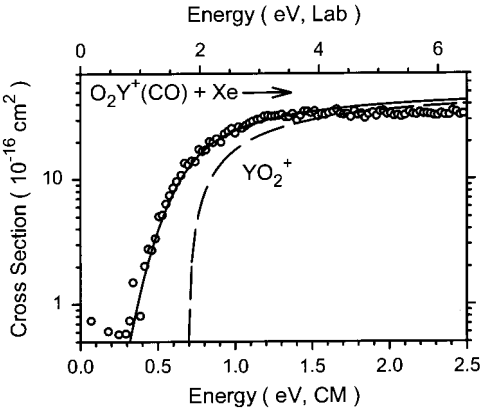

Figure 6. Product cross sections for $O_2Y^+(CO) + Xe$ as a function of collision energy in the center-of-mass frame (lower *x* axis) and laboratory frame (upper *x* axis). The dashed line is the model of eq 2 with the optimized parameters listed in Table 3 for the CID process. The solid line shows this model convoluted with the experimental energy distributions.

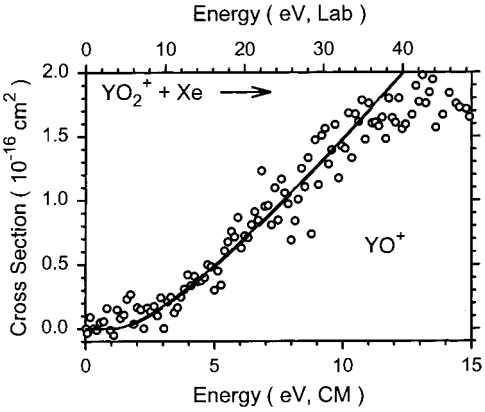

Figure 7. Product cross sections for $YO_2^+ + Xe$ as a function of collision energy in the center-of-mass frame (lower *x* axis) and laboratory frame (upper *x* axis). The dashed line is the model of eq 2 with the optimized parameters listed in Table 3 for the CID process. The solid line shows this model convoluted with the experimental energy distributions.

structure and that O_2 elimination is inefficient. The YO^+ cross section is relatively noisy and rises very slowly from an apparent threshold near 2 eV. As a consequence, the analysis of the energy dependence of this cross section is not particularly well-defined, leading to a wide range of threshold energies consistent with the data (Table 3). The final E_0 value of 1.4 ± 0.5 eV is within experimental error of the more precise value of $D_0(OY^+-O) = 1.76 \pm 0.16$ eV given in Table 1.[25] The data can easily be reproduced well using eq 2 and this bond energy for E_0.

IV. Discussion

An important consideration in the systems studied here is the electronic states of the metal, metal monoxide, and metal dioxide cations. The ground state of Y^+ is $^1S(5s^2)$,[44] with low lying excited states (in eV) at 0.10 (a^3D, $5s^14d^1$), 0.41 (a^1D, $5s^14d^1$), 0.99 (a^3F, $4d^2$), 1.72 (a^3P, $4d^2$), and 1.84 (b^1D, $4d^2$) above the ground state. The ground state of YO^+ is known to be $^1\Sigma^+$ ($1\sigma^21\pi^4$).[45] To our knowledge, no work has been done to ascertain the energetics of excited states of YO^+. Overall, these considerations show that the reaction of ground-state $Y^+(^1S)$ with $CO_2(^1\Sigma_g^+)$ to form ground-state $YO^+(^1\Sigma^+)$ + $CO(^1\Sigma^+)$ products is spin-allowed. This is one reason that the exothermic reaction 3 is efficient (Figure 1), occurring on two-thirds of all collisions. In addition, the reverse reaction, process 7, begins promptly at its thermodynamic threshold and is also fairly efficient considering that it is endothermic (Figure 2).

In contrast, the exothermic reaction of $YO_2^+ + CO$ ($^1\Sigma^+$) to form YO^+ ($^1\Sigma^+$) + CO_2 ($^1\Sigma_g^+$), process 11, exhibits a threshold and its endothermic reverse, process 9, appears to have a threshold above the thermodynamic value. In our other studies of reaction 1,[1-4] unusual kinetic energy behavior could be shown to be consequences of spin-conservation and the resultant formation of excited electronic states. Therefore, we carefully consider the possibility that one explanation for the elevated thresholds observed is that reaction 9 is spin-forbidden to form a ground-state triplet YO_2^+. The ground state for the metal dioxide cation is unknown theoretically or experimentally, but theoretical calculations indicate that the YO_2 neutral molecule has a $^2\Sigma^+$ ground state.[46] Therefore the YO_2^+ cation probably has a triplet or singlet ground state. Reactions 9 and 11 are spin-allowed only if the spin state of the dioxide cation is a singlet, not a triplet.[47] Therefore, it is possible that reaction occurs preferentially to form an excited singlet state of the YO_2^+ product lying 0.85 ± 0.34 eV above a ground-state triplet. For the reverse exothermic reaction, the delayed threshold would then need to be associated with formation of a triplet excited state of YO^+ lying 4.07 ± 0.19 eV above the singlet ground state. This seems an excessively large value for the lowest triplet state, which would correspond to promotion of a bonding 1π electron from the $^1\Sigma^+(1\sigma^21\pi^4)$ ground state into a nonbonding 2σ or 1δ orbital. In ZrO^+, we speculatively assigned a 2.93 ± 0.14 eV energy to the 1π to 1δ orbital excitation,[3] an assignment made plausible by a comparable value, 3.34 eV, calculated for this same excitation in the isoelectronic YO molecule.[48] It is possible that the 4.07 ± 0.19 eV energy could correspond to a 1π to 2π excitation, yielding a $^3\Phi/^3\Sigma^-$ state for YO^+. A similar excitation energy of 3.93 ± 0.06 eV was speculatively assigned to this same orbital promotion for MoO^+.[4] However, it is hard

(43) Aristov, N.; Armentrout, P. B. *J. Phys. Chem.* **1986**, *90*, 5135.
(44) Moore, C. E. *Atomic Energy Levels*; US GPO Circular No. 467; Washington, DC, 1952.
(45) Linton, C.; Simard, B.; Loock, H.-P.; Rothschopf, G.; Gunion, B.; Morse, M. D. Manuscript in preparation.
(46) Siegbahn, P. E. M. *J. Phys. Chem.* **1993**, *97*, 9096.
(47) It should also be mentioned that if YO_2^+ has a singlet ground state, then reaction 8 is spin-forbidden. In which case, the elevated threshold observed for this process could be associated with the formation of an excited triplet state of YO_2^+ in a spin-allowed reaction.
(48) Langhoff, S. R.; Bauschlicher, C. W., Jr. *J. Chem. Phys.* **1988**, *89*, 2160.

to understand why these latter states would be formed while the lower lying triplet states would not.

An alternate and more likely explanation is a barrier in excess of the asymptotic energy of the $YO_2^+ + CO$ species that is common to both reactions 9 and 11. This is measured most precisely from our analysis of the cross section for reaction 11 as 0.38 ± 0.11 eV, but this roughly agrees within combined experimental errors with the much less precise value obtained for the reverse process, 0.85 ± 0.34 eV. We believe that the origin for such a barrier is probably related to the potential energy surfaces for dissociation of CO_2 ($^1\Sigma_g^+$). Bond cleavage to form CO ($^1\Sigma^+$) + O (^{3}P) ground-state species is spin-forbidden, while the spin-allowed dissociation asymptote, CO ($^1\Sigma^+$) + O (^{1}D), lies 1.97 eV higher in energy. Hence there is a barrier in excess of the OC−O bond dissociation energy of 5.453 eV that must be overcome to remove O from CO_2 in a spin-allowed process. The barrier observed in reactions 9 and 11 is probably a reflection of the complex potential energy surface associated with oxygen atom abstraction from CO_2. No such barrier is confronted in the reaction of Y^+ with CO_2 because of the much stronger YO^+ bond compared to the YO_2^+ bond.

It is also interesting to examine the trends in the carbonyl bond energies to Y^+, YO^+, and YO_2^+. Table 1 shows that the value for Y^+−CO, 0.31 ± 0.11 eV, is less than half that for OY^+−CO and O_2Y^+−CO. The easiest way of rationalizing this result is simply to note that CO bonds primarily by donating a pair of electrons to the 5s orbital on the metal center. The ground state of YCO^+ is $^1\Sigma^+$ and involves a mixture of binding to the ^{1}S ($5s^2$) ground state and ^{1}D ($5s^14d^1$) excited state of Y^+.[42] Because the 5s-like orbital is occupied in YCO^+, this leads to a relatively weak bond. The lowest lying excited state of Y^+ where the 5s orbital is empty, ^{3}F ($4d^2$), lies 0.99 eV higher in energy, such that this state does not lead to the ground state for YCO^+. In contrast, Zr^+, which has a low lying $4d^3$ state, and Nb^+, which has $4d^4$ ground state, have substantially larger bond energies to CO: 0.80 ± 0.10 and 0.99 ± 0.05 eV, respectively.[2,3] Bonding between Y^+ and O primarily utilizes the metal 4d orbitals such that the 5s-like orbital is essentially empty in YO^+ and YO_2^+. This permits a much stronger bond with CO, comparable to that for Zr^+ and Nb^+. This bonding picture is consistent with similarly strong bond energies, ranging from 0.80 ± 0.08 to 1.11 ± 0.05 eV, for binding CO to ZrO^+, ZrO_2^+, NbO^+, NbO_2^+, MoO^+, and MoO_2^+.[2−4]

Acknowledgment. This research is supported by the National Science Foundation, Grant No. 9530412.

IC981117F